Aerospace Science and Technology 40 (2015) 128–137

Contents lists available at ScienceDirect

Aerospace Science and Technology

www.elsevier.com/locate/aescte

A GPC-based auto-throttle with robust fuel-efficient operation in 4D flights ☆

Dimitrios Dimogianopoulos [a,*], Vangelis Petratos [b], Fotis Kopsaftopoulos [b,1], Spilios Fassois [b]

[a] Technological Education Institute of Piraeus, 122 44 Egaleo, Greece
[b] Stochastic Mechanical Systems & Automation (SMSA) Laboratory, Department of Mechanical Engineering & Aeronautics, University of Patras, GR 265 04 Patras, Greece

ARTICLE INFO

Article history:
Received 12 March 2014
Received in revised form 30 October 2014
Accepted 11 November 2014
Available online 18 November 2014

Keywords:
Model predictive control
Generalized predictive control
Auto-throttle
4D flights
ARX models
Specific fuel consumption

ABSTRACT

This paper introduces a novel auto-throttle controller designed for robust and fuel-efficient operation under changing flight conditions in four-dimensional (4D) flight trajectories (3D + time). Following typical receding horizon techniques, the throttle values are obtained by optimizing the predicted response of the system over future time intervals. The novelty is two-fold: First, the controller is designed to achieve a user-defined, realistic reference value for the aircraft Specific Fuel Consumption (SFC), while maintaining the nominal safety margins during the 4D flights. Second, the throttle commands result from a closed-form expression with minimal computational effort, thus simplifying the proposed auto-throttle's on-board implementation. Tests against a conventional PID-based auto-throttle illustrate the current controller's superior robustness under challenging flight conditions (turbulence).

1. Introduction

One of the basic targets of Air Traffic Management (ATM) is the implementation of the Four-Dimensional (4D) flight concept. In essence, the 4D flight relies on the definition of Four-Dimensional Way Points (4DWPs), which relate the 3D aircraft position to corresponding time points (T) throughout the flight. The succession of 4DWPs define the Four-Dimensional Contracts (4DCos), which are specific to the given aircraft flight. Ensuring flight safety in 4DCos is a capital task, which is based on the introduction of "safety bubbles". These define the maximum allowable cross-track and along-track deviations of the aircraft from its current position before conflicts with other aircraft occur. Although several new constraints related to the strict aircraft 4DCo compliance are introduced, the 4DCo concept provides new opportunities for a safer, environmentally friendlier and less human-involved management of the airspace [13].

From an ATM point of view, the 4DCo concept has been extensively studied, among others, for optimizing the fuel efficiency (consumption/emissions) on a given transition between way points. The first results appeared almost 3 decades ago, with representative efforts including [23] and [4], whereas recent results may be found in [8] and [9]. The aim of these studies has always been to deliver fuel-optimal trajectories during either climb/descend flight phases as in [4,23], or constant altitude flights possibly in presence of horizontal winds as in [8,9]. In [23] and [4] the trajectory is obtained via the minimization of the (modeled) Direct Operating Cost (DOC) of the given aircraft and flight, which essentially represents the combined costs of the fuel consumed and the flight duration. In [8] and [9] the trajectory results from solving a singular optimal control problem with the constraint of a fixed arrival time and under the effects of horizontal winds and changing aircraft mass. Following this approach, the optimal cruise speed and the optimal control required for meeting the time constraints in the considered case are delivered. Nevertheless, even when a fuel-optimal succession of 4DWPs is defined for a given trajectory, the aircraft should move from one such 4DWP to the next as safely and efficiently as possible: In other words, aircraft fuel use and safety are also related to developing suitable auto-throttle strategies achieving both 4DCo compliance and optimal (in some sense) efficiency.

☆ An early version of this work has been presented in the 9th Asian Control Conference (ASCC 2013) Istanbul, June 23–26, 2013.

* Corresponding author. Tel.: +30 210 538 1183.
E-mail address: dimogian@teipir.gr (D. Dimogianopoulos).

[1] F. Kopsaftopoulos is currently with Structures & Composites Laboratory (SACL), Department of Aeronautics and Astronautics, Stanford University, Stanford, CA 94305, United States.

http://dx.doi.org/10.1016/j.ast.2014.11.002
1270-9638/

An extensive description of engine control strategies under multiple (mechanical or aerothermal) constraints may be found in [24]. Therein, the basic principles of operation and the limitations for each engine component are reviewed, and various control strategies respecting the typical requirements for sensors and actuators are given. On the other hand, the control objective is the effective use of the engine for better fuel consumption and part life, rather than the satisfaction of critical 4DCo-related constraints such as the aircraft's position in the safety bubble. Similar efforts for designing controllers which take into account multiple objectives (one of which is the fuel use) may be found in [22]. There, the response time during the engine's acceleration/deceleration and the fuel consumption are considered as objective functions, whereas a Wiener model with experimentally estimated parameters represents the gas turbine engine. The controller gains are tuned by Particle Swarm Optimization (PSO) techniques, meaning that the on-line gain computation depends on the PSO convergence rate. Again, the control objective is the effective fuel use and the protection of physical limitations of the engine components. In other words, most engine control strategies consider the effective fuel use as one of several other mechanical- (rather than flight-) related objectives that have to be achieved. An exception may be found in [3], with the engine control strategy involving constraints relevant to both performance (thrust, specific fuel consumption) and operability (costs, in-flight mishaps) factors. Due to the existence of constraints (among others) on the aircraft state, the problem is formulated in a nonlinear predictive control form, meaning that its solution (hence, the control values) must be obtained via an iterative procedure. The on-board computation of control values might, thus, be compromised.

Fuel efficiency and overall optimization of jet engines have often been linked to SFC minimization [19,20]. Even though measuring the SFC is still a controversial subject, it is widely accepted that the SFC may be estimated either from thermodynamic models [15], or indirectly by thrust estimation via physics-based models [10] or from data provided by the Full Authority Digital Engine Control (FADEC) [18], as will be discussed later on. In any case, optimizing engine control for minimal SFC seems already feasible, and may even be executed on-line [19,20] if engine performance charts are available.

This paper aims at introducing an auto-throttle controller design, which leads to obtaining aircraft 4DCo compliance, while simultaneously achieving a (realistic) user-defined reference SFC value. In other words, both safety and effective fuel use (in the previously described sense) are objectives to be fulfilled by the control strategy. The controller design is based on typical receding horizon techniques as in [3], with control values resulting from optimizing the predicted system response over future time intervals. It essentially exploits a variant of Model Predictive Control (MPC) referred to as Generalized Predictive Control (GPC) as proposed by Clarke et al. in [6] and extensively analyzed in [5]. The GPC is a special MPC case, which provides a closed-form solution to the control problem under the condition that the system can be modeled using linear representations. For a brief but comprehensive analysis (and list of references) of the MPC methodologies, the reader is referred to [16].

The novelty of the current scheme is that the system response is now related to fuel efficiency in terms of SFC (as in [18–20]) and to flight safety in terms of the aircraft position inside the 4DCo safety bubble. The latter corresponds here to an operability objective [3] and, to the best of the authors' knowledge, it has never been used as such before. The advantage of the proposed controller is that the control values result from solving a *linear* predictive control problem. This is feasible for two reasons: First, the constraint related to the aircraft's 4DCo compliance is defined as an objective in the cost index of the predictive control problem (see Subsection 2.3). Hence, no explicit constraints in the (generalized predictive) control problem (as in [21]) are used, and no iterative techniques for computing the control solution are necessary. Second, with respect to the SFC objective, a linear AutoRegressive with eXogenous excitation (ARX) representation of the relationship between throttle command and SFC may be identified, if the latter is available or can be dependably estimated. The use of ARX representations for modeling engine dynamics has often proved effective [7], and helps formulating a GPC problem (as will be shown later on), whose solution admits an analytical closed-form. Thus, computing the control values is an instant, real-time procedure, which could be easily performed on-board without inducing computational burden. The proposed controller is implemented on a Boeing 737 simulation software and tested via several flights conducted under normal or degraded conditions. Comparisons in such conditions are made with a PID controller, tuned in the (traditional) sense of achieving 4DCo compliance. The robustness advantage in favor of the currently proposed controller seems quite significant.

The paper is organized as follows: Section 2 presents the GPC problem formulation and provides the step by step analysis of the control strategy along with the theoretic analysis of closed loop stability. In Section 3, the proposed controller is implemented and tested in a simulated Boeing 737, whereas its performance is evaluated against a classical PID scheme under challenging environmental conditions. Finally, conclusions are drawn in Section 4.

2. Principles of controller design

In terms of controller design, a typical starting point is the availability of an accurate representation of the system dynamics. An accurate system model may be derived by using physical principles, especially when the system structure is perfectly known and/or easy to be studied. Alternatively, stochastic or deterministic models may be identified for successfully representing the macroscopic system behavior between desired Input and Output (I/O) channels of the system without using any knowledge of its internal structure. In the current case, the relationship between the throttle command and the resulting aircraft SFC has to be modeled. Given the complexity of the underlying (thermodynamic, mechanical and so on) processes, effort is put towards identifying a (possibly simple) linear stochastic ARX time series model for achieving an accurate and robust representation of these dynamics.

Once the ARX model is identified, the control problem may be formulated in a GPC framework. This means that specific attributes of the system behavior are predicted over future time intervals and compared with desired relevant reference values. Mathematically, this comparison admits the form of a quadratic criterion, whose minimization yields the control values required for achieving the reference values set. As will become obvious later on, the problem formulation and solution is made easier by modeling the relationship between the throttle command and the SFC via a linear ARX representation. This results in an easy and real-time fast computation of the required control values. In the current study, two main system attributes are involved in the MPC problem formulation:

(i) The SFC values, which should achieve some (realistic) user-defined references; this is the first of the control objectives and is taken into account by the Basic Minimization Criterion (BMC), which penalizes the mean square error between predicted (by the ARX model) and desired SFC values.
(ii) The aircraft compliance with the allocated 4DCo, which is the second control objective; this is accounted for by an extra term added to the BMC, which penalizes the aircraft deviations from the 4D trajectories imposed by the 4DCo.

Details on the ARX identification and the GPC problem formulation are given in the following subsections.

2.1. Modeling of the relationship between throttle and SFC

The modeling of the relationship between throttle command and engine SFC may be based on a discrete-time stochastic model obtained via standard identification procedures [17]. In this study, an ARX(na, nb) representation is considered, which admits the form [17]:

$$y[t] + \sum_{i=1}^{na} a_i \cdot y[t-i] = \sum_{i=0}^{nb} b_i \cdot u[t-i] + w[t] \tag{1}$$

Using the backshift operator ($\mathcal{B}^i \cdot y[t] \triangleq y[t-i]$), (1) becomes:

$$A(\mathcal{B}) \cdot y[t] = B(\mathcal{B}) \cdot u[t] + w[t], \quad w[t] \sim \text{iid}\, \mathcal{N}\big(0, \sigma_w^2\big) \tag{2}$$

$$A(\mathcal{B}) = 1 + a_1 \cdot \mathcal{B} + \ldots + a_{na} \cdot \mathcal{B}^{na}$$

$$B(\mathcal{B}) = b_0 + b_1 \cdot \mathcal{B} + \ldots + b_{nb} \cdot \mathcal{B}^{nb} \tag{3}$$

with t designating the normalized discrete time[2] ($t = 1, 2, \ldots$), and $y[t]$, $u[t]$ the measured output (SFC) and control input (throttle command) signals, respectively. The AutoRegressive (AR) and eXogenous (X) orders are noted as na and nb, respectively, whereas $A(\mathcal{B}), B(\mathcal{B})$ are the AR and X polynomials, respectively. The signal $w[t]$ is uncorrelated (white) with zero mean and variance σ_w^2. It coincides with the model based one-step-ahead prediction error, and is uncorrelated with the excitation $u[t]$. The symbol $\mathcal{N}(\cdot,\cdot)$ designates Gaussian distribution with the indicated mean and variance, and iid stands for identically independently distributed. The model admits the linear regression form:

$$y[t] = \boldsymbol{\phi}^T[t] \cdot \boldsymbol{\theta} + w[t] \tag{4}$$

with $\boldsymbol{\phi}[t] = [-y[t-1], \ldots, -y[t-na], u[t], \ldots, u[t-nb]]^T$ and $\boldsymbol{\theta} = [a_1, \ldots a_{na}, b_0 \ldots b_{nb}]^T$. The estimation of the parameter vector $\boldsymbol{\theta}$ is based on the measured input and output data and is achieved by minimizing Ordinary Least Squares (OLS) or Weighted Least Squares (WLS) criteria [17, pp. 8–9].

As previously stated, obtaining values for the SFC depends on the possibility of estimating thrust. In general, thrust estimation may be performed either by using physics-based thermodynamic models as stand-alone thrust estimators [15], or as the basis for designing observers for on-line estimation [10]. Again, thrust may be estimated from data either collected or estimated by the digital avionics and communicated to FADEC system, as claimed in [18]. Note that choosing to focus on SFC for controller design purposes instead of, for instance, the pure fuel flow is due to the fact that the SFC perfectly describes fuel efficiency, since the fuel usage is related to the thrust produced. The importance of SFC in engine development is also highlighted by claims that its reduction by 4% is a reason for implementing a new engine design [20]. For the same reasons, algorithms exploiting engine performance charts and attempting to optimize engine control on-line with respect to the SFC have already been reported [19,20].

2.2. The basic minimization criterion

The Basic Minimization Criterion (BMC) penalizes the mean square error between predicted SFC and reference value at each time instant. The identified ARX model is used for predicting SFC values over a j-step-ahead prediction horizon based on the current and past throttle commands. Subsequently, the BMC minimization results in the future values of the control input (throttle command), which will achieve SFC values close to those set as references. Consider the Diophantine Equation (see [6]):

$$E_j(\mathcal{B}) \cdot A(\mathcal{B}) + \mathcal{B}^j \cdot F_j(\mathcal{B}) = 1, \tag{5}$$

with $E_j(\mathcal{B})$ and $F_j(\mathcal{B})$ polynomials uniquely defined for the given $A(\mathcal{B})$, and j the number of future steps forming the prediction horizon. The optimal j-th-step-ahead predictor involving the measured output data up to time t and some $u[t+j]$ for $j > 1$ is obtained as [6]:

$$\widehat{y}[t+j|t] = G_j(\mathcal{B}) \cdot u[t+j] + F_j(\mathcal{B}) \cdot y[t], \tag{6}$$

where

$$G_j(\mathcal{B}) \triangleq E_j(\mathcal{B}) \cdot B(\mathcal{B}). \tag{7}$$

Denoting the coefficients of the polynomials $G_j(\mathcal{B})$ and $F_j(\mathcal{B})$ as $g_{j,0}, \ldots, g_{j,j-1}$ and $f_{j,0}, \ldots, f_{j,na-1}$, respectively, the vector of j estimated future outputs may be expressed as:

$$\widehat{\boldsymbol{y}}_t = \boldsymbol{G} \cdot \boldsymbol{u}_t + \boldsymbol{p}_t \tag{8}$$

where:

$$\widehat{\boldsymbol{y}}_t = \big[\widehat{y}[t+1] \ldots \widehat{y}[t+j]\big]^T, \tag{9a}$$

$$\boldsymbol{u}_t = \big[u[t+1] \ldots u[t+j]\big]^T, \tag{9b}$$

$$\boldsymbol{G} = \begin{bmatrix} g_{1,0} & \cdots & 0 \\ \vdots & \ddots & \vdots \\ g_{j,j-1} & \cdots & g_{j,0} \end{bmatrix}, \tag{9c}$$

$$\boldsymbol{p}_t = \begin{bmatrix} g_{1,nb} & \cdots & g_{1,1} & f_{1,na-1} & \cdots & f_{1,0} \\ \vdots & \ddots & \vdots & \vdots & \ddots & \vdots \\ g_{j,j-1} & \cdots & g_{j,0} & f_{j,na-1} & \cdots & f_{j,0} \end{bmatrix} \cdot \begin{bmatrix} u[t-nb+1] \\ \vdots \\ u[t] \\ y[t-na+1] \\ \vdots \\ y[t] \end{bmatrix}. \tag{9d}$$

Now, consider the following quadratic criterion:

$$J_t = \sum_{i=1}^{j} \big(y[t+i] - r[t+i]\big)^2 + \mu \cdot \sum_{i=1}^{j} \big(u[t+i] - u[t+i-1]\big)^2. \tag{10}$$

The first term of the criterion penalizes the squared difference between the system's actual (measured/estimated) SFC and a reference (desired) SFC signal $\boldsymbol{r}_t = [r[t+1] \ldots r[t+j]]^T$. The second term penalizes the squared first differences of the future input control (throttle) commands, with μ being a weighting constant. The term is often used when the model that predicts the output (here, the ARX model) has non-minimum phase characteristics [16, p. 808]. It penalizes any abrupt activity of the throttle command, allowing for smoother throttle operation. As shown in [11], the last sum can be expressed as $\boldsymbol{D} \cdot \boldsymbol{u} - \boldsymbol{I_0}$, where $\boldsymbol{I_0} = [1, 0, \cdots, 0]^T$ and:

[2] The absolute time is $(t-1)T_s$, where T_s stands for the sampling period.

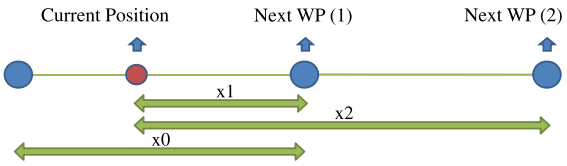

Fig. 1. The aircraft desired speed at the current condition depends on WP(1) and WP(2). A component-speed is calculated for each of these two WPs, by dividing its distance from the aircraft with the remaining time-to-arrival. The desired speed is a linear combination of the two component speeds.

$$\boldsymbol{D} = \begin{bmatrix} 1 & 0 & 0 & \cdots & 0 \\ -1 & 1 & 0 & \cdots & 0 \\ 0 & -1 & 1 & & \vdots \\ \vdots & & \ddots & \ddots & 0 \\ 0 & \cdots & 0 & -1 & 1 \end{bmatrix}.$$

Hence, the quadratic criterion may be expressed as:

$$J_t = (\boldsymbol{G}\cdot\boldsymbol{u}_t + \boldsymbol{p}_t - \boldsymbol{r}_t)^T \cdot (\boldsymbol{G}\cdot\boldsymbol{u}_t + \boldsymbol{p}_t - \boldsymbol{r}_t) + \mu\cdot(\boldsymbol{D}\cdot\boldsymbol{u}_t - \boldsymbol{I_0})^T \cdot (\boldsymbol{D}\cdot\boldsymbol{u}_t - \boldsymbol{I_0}). \quad (11)$$

As J_t is a quadratic function of the unknown control vector $\boldsymbol{u}_t$ (yet to be estimated), it can be minimized by setting to zero its partial derivative with respect to $\boldsymbol{u}_t$. This yields:

$$\boldsymbol{u}_t = \left(\boldsymbol{G}^T\boldsymbol{G} + \mu\cdot\boldsymbol{D}^T\boldsymbol{D}\right)^{-1}\cdot\left(\mu\cdot\boldsymbol{D}^T\boldsymbol{I}_0 + \boldsymbol{G}^T(\boldsymbol{r}_t - \boldsymbol{p}_t)\right). \quad (12)$$

Note that this is a closed-form solution of the control value $\boldsymbol{u}_t$. Hence, the current scheme features a significant advantage in terms of computational burden, since it does not require iterative procedures for computing the control solution. Consequently, no extra on-board computational effort (nor time) is required for computing the values of $\boldsymbol{u}_t$, making the proposed controller easier to implement in real-time applications.

2.3. Extensions to the basic minimization criterion for 4DCo compliance

In order for the GPC scheme to take into account the assigned 4DCo and ensure aircraft compliance to it, an extra term is added to the BMC. The criterion then admits the following form:

$$J_t^{\mathrm{EXT}} = J_t + \lambda_0[t]\cdot\sum_{i=1}^{j} u^2[t+i] + \lambda_1[t]\cdot\sum_{i=1}^{j}\big(1-u[t+i]\big)^2 \quad (13)$$

with $\lambda_0[t]$ and $\lambda_1[t]$ being positive time-varying weighting factors. Note that these factors are updated *only after* the "current" control value is computed, and remain constant during the minimization of J_t^{EXT}, from which the computation of the "next" control value is obtained. The first term penalizes the squared control signal values: higher $\lambda_0[t]$ values should result in throttle commands of lower magnitudes. Similarly, the second term penalizes the squared differences between the control signal and unity: higher $\lambda_1[t]$ values yield increased throttle command magnitudes, as will be explained later on. The selection of unity stems from the fact that the throttle commands are in the $[0, 1]$ interval.

In order to compute $\lambda_0[t]$ and $\lambda_1[t]$, a desired aircraft ground speed must be defined. This speed is a linear combination of two component ground speeds, which are associated to the distances from (and the times-of-arrival at) the two WPs ahead from the current aircraft position, namely WP(1) and WP(2) depicted in Fig. 1. The first component speed $v_1[t]$ is related to WP(1), and is computed by dividing the distance $x_1[t]$ with the estimated time-to-arrival (Fig. 1). The same holds for the second component speed $v_2[t]$, which is computed by dividing the distance $x_2[t]$ with the estimated time-to-arrival related to WP(2). The desired

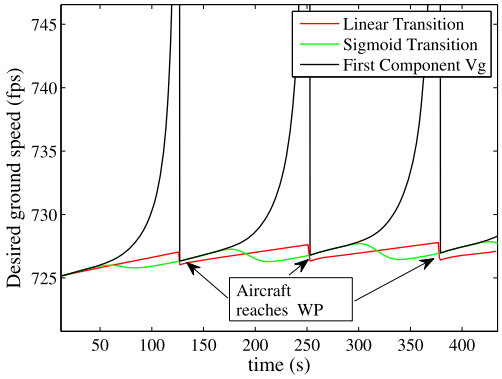

Fig. 2. Methods for defining the desired aircraft ground speed. (For interpretation of the references to color in this figure legend, the reader is referred to the web version of this article.)

ground speed results from linearly combining these two component ground speeds with weights $W[t]$ and $1 - W[t]$ that come from a sigmoid function $W[t] = (erf(8\cdot(x[t]-0.5))+1)/2$. The term $erf(\cdot)$ is the Gauss Error Function [1, pp. 100–111], whereas $x[t]$ is the distance to be covered until the next WP and is equal to $x_1[t]$ over the total distance $x_2[t]$ between two WPs (Fig. 1). These weights and the sigmoid function produce a smooth transition from the first component ground speed to the second, as the aircraft reaches the next WP, as indicated by the green line in Fig. 2. If a linear (instead of sigmoid) transition is used, the desired ground speed is not continuous when the aircraft changes WP (red line). Note, also, that using only the first component as the desired speed is not an acceptable solution: Had this been the case, the desired speed would become either very large or small when reaching the WP, as indicated by the black line in Fig. 2. This is the reason for defining the desired speed by means of a linear combination of the two components.

A step-by-step procedure for the determination of the desired ground speed is outlined below:

Step 1: At each time instant calculate the two component ground speeds $v_1[t]$, $v_2[t]$ using the distances $x_1[t]$ and $x_2[t]$ and the estimated times-of-arrival with respect to waypoints WP(1) and WP(2), respectively (see Fig. 1).

Step 2: Using the ratio of the distance $x_1[t]$ to be covered until the next WP (WP(1) in Fig. 1) over the total distance $x_2[t]$ (WP(2) in Fig. 1), designated as $x[t] = x_1[t]/x_2[t]$, calculate the weights $W[t]$ and $1 - W[t]$ using the sigmoid function $W[t] = (erf(8\cdot(x[t]-0.5))+1)/2$.

Step 3: Calculate the desired speed $v_d[t]$ as a linear combination of the two component ground speeds $v_{d_1}[t]$, $v_{d_2}[t]$ with weights equal to $W[t]$ and $1 - W[t]$, that is $u_d[t] = W[t]\cdot v_1[t] + (1 - W[t])\cdot v_2[t]$.

As seen, $W[t]$ is suitably defined for normalizing the input–output to the zero-one interval. Factor 8 is empirically derived and allows for regulating the sigmoid's curvature. The aim is to achieve a trade-off between smooth transition and flatness of the sigmoid limits, as shown in Fig. 3. A curvature factor of 4 (black line) produces a smooth transition, but without flat enough sigmoid limits. The flatness of the limits is important in order to avoid having discontinuities when the aircraft reaches the next WP, as discussed previously. A curvature factor of 12 (red line) produces flat enough sigmoid limits, but also a sharp transition leading to sudden changes in the desired ground speed if the two components differ significantly. Finally, a curvature factor of 8 (green line) produces a smooth transition and appropriately flat sigmoid limits.

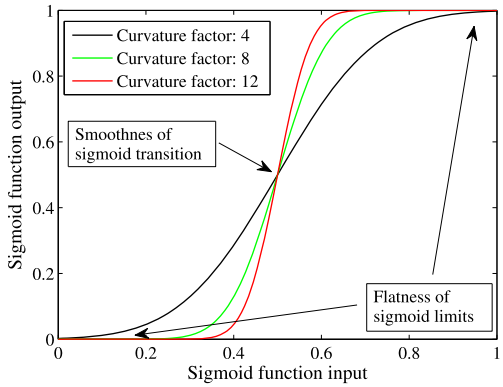

Fig. 3. The sigmoid function for various curvature factors. (For interpretation of the references to color in this figure legend, the reader is referred to the web version of this article.)

Given the desired ground speed, the weighting factors $\lambda_0[t]$ and $\lambda_1[t]$ may now be defined as:

$$\lambda_0[t] = c_a \cdot e^{c_b(v_{tr}[t]-v_d[t])}, \tag{14a}$$

$$\lambda_1[t] = c_a \cdot e^{c_b(v_d[t]-v_{tr}[t])} \tag{14b}$$

where c_a, c_b are user defined tuning parameters and $v_d[t]$, $v_{tr}[t]$ the desired and actual aircraft ground speeds, respectively. According to (13), penalty is imposed on any (potential) non-compliance of the aircraft to its allocated 4D contract using λ_0 and λ_1 (with the argument t dropped for convenience). The relevant terms impose penalties according to whether the aircraft is "late" or "early" with respect to its nominal 4D position as set by the allocated 4D contract. When the aircraft is "early", λ_0 increases, and the magnitude of the control value is penalized. At the same time, λ_1 decreases and the associated term becomes less significant, because the danger of achieving full-throttle (that is $\boldsymbol{u}_t = 1$) is minimal, given that the aircraft is early and the throttle should be reduced. The opposite reasoning is valid when the aircraft is "late" with respect to its allocated 4D position. Finally, if the actual speed is close to the desired one, both λ_0 and λ_1 will admit small values (close to c_a). Then, the SFC-related part J_t in (13) becomes dominant, meaning that the control values will be computed primarily for achieving the desired SFC values rather than 4DCo compliance. The latter is ensured by the fact that if the actual speed is equal to the desired one, the aircraft *will* arrive at the next WP on time. Adding the extension terms to the BMC, the quadratic criterion (13) becomes:

$$J_t^{\text{EXT}} = J_t + \lambda_0[t] \cdot \boldsymbol{u}_t^T \boldsymbol{u}_t + \lambda_1[t] \cdot (\boldsymbol{I}_e - \boldsymbol{u}_t)^T (\boldsymbol{I}_e - \boldsymbol{u}_t), \tag{15}$$

where $\boldsymbol{I}_e = [1 \ldots 1]^T$. Note that by using λ_0 and λ_1 in J_t^{EXT}, the 4DCo compliance is achievable *without introducing explicit constraints* in the control problem. Hence, setting the partial derivative with respect to $\boldsymbol{u}_t$ of J_t^{EXT} to zero yields the closed-form solution:

$$\begin{aligned}\boldsymbol{u}_t = &\big(\boldsymbol{G}^T\boldsymbol{G} + \mu \cdot \boldsymbol{D}^T\boldsymbol{D} \\ &+ \big(\lambda_0[t] + \lambda_1[t]\big) \cdot \boldsymbol{I}\big)^{-1} \cdot \big(\mu \cdot \boldsymbol{D}^T\boldsymbol{I}_0 \\ &+ \lambda_1[t] \cdot \boldsymbol{I}_e + \boldsymbol{G}^T \cdot (\boldsymbol{r}_t - \boldsymbol{p}_t)\big),\end{aligned} \tag{16}$$

where $\boldsymbol{I}$ is the identity matrix. The GPC-based auto-throttle block diagram is depicted in Fig. 4.

2.4. Closed loop stability analysis

The stability analysis of the controlled closed loop system will be based on qualitative characteristics of the open-loop system, because specific knowledge on its input/output relationships (transfer functions, for instance) is unavailable. The relationship between the throttle command and the resulting ground speed is initially considered.

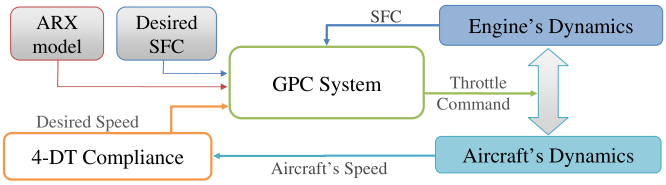

Fig. 4. The GPC-based auto-throttle block diagram.

Fig. 5 presents the negative-feedback closed loop formed by the proposed controller block and that corresponding to the open-loop relationship between throttle and ground speed (block F). In principle, the desired ground speed $v_d[t]$ is compared with the actual one designated as $v_{tr}[t]$, and the error $e[t] = v_d[t] - v_{tr}[t]$ is used along with (16) to provide the throttle command $\boldsymbol{u}_t$. The theoretic transfer function of the block F is unknown. Nevertheless, given that the (commercial) aircraft systems are designed to be stable and as linear as possible, it may safely be assumed that the transfer function of block F is stable and has a finite static gain γ_F. For instance, the system response in terms of ground speed to a step throttle input may be seen in Fig. 5, and resembles to the step response of a first-order stable system. The transfer function parameters are approximately constant inside (limited) areas of the aircraft location in the flight envelope, and under comparable external disturbances. Naturally, even if the transfer function parameters admit different (constant) values in different flight envelope locations, the stability of the relationship between throttle and ground speed and the existence of some finite static gain γ_F will be valid.

In order to analyze the stability of this closed loop, two cases can be distinguished. The first case corresponds to the possibility of $e[t] < 0$, which means that the aircraft flies faster than it should, with respect to its allocated 4D contract. Then, each time a new throttle command $\boldsymbol{u}_t$ is to be computed, from (14a) λ_1 diminishes exponentially with $e[t]$ whereas λ_0 grows, and (16) shows that $\boldsymbol{u}_t$ will always decrease. In that case, the aircraft will fly slower and $e[t]$ will continue admitting negative values, but towards zero. Thus $e[t]$ cannot grow unbounded in this case. This conclusion is also valid if disturbances and (modeling or other) uncertainties are present in the closed loop of Fig. 5. Then, the worst scenario for the case considered would be that the aircraft flies even faster with respect to the given throttle command, so that $e[t] < 0$ with $|e[t]|$ increasing. This would translate in even smaller throttle commands, so that the aircraft would fly slower and $e[t]$ would ultimately decrease or at least stay bounded.

The second case corresponds to the possibility of $e[t] > 0$, which means that the aircraft flies slower than it should with respect to its 4D contract. At a given time t, let $e[t] = \epsilon$ with ϵ a small ("epsilon-esque") positive number. Then, using (14a) and (16) the throttle command will be (approximately) equal to the following value:

$$\begin{aligned}\boldsymbol{u}_t = &\big(\boldsymbol{G}^T\boldsymbol{G} + \mu \cdot \boldsymbol{D}^T\boldsymbol{D} \\ &+ 2 \cdot c_a \cdot \boldsymbol{I}\big)^{-1} \cdot \big(\mu \cdot \boldsymbol{D}^T\boldsymbol{I}_0 + c_a \cdot \boldsymbol{I}_e \\ &+ \boldsymbol{G}^T \cdot (\boldsymbol{r}_t - \boldsymbol{p}_t)\big) = \boldsymbol{u}^*.\end{aligned} \tag{17}$$

The controller block in Fig. 5 will have a gain $\gamma_c = \epsilon^{-1} \cdot \|\boldsymbol{u}^*\|$, which is, understandably, "large". Now recall that by virtue of the small gain theorem (see [14] and [2]), the condition of $\gamma_c \cdot \gamma_F < 1$ is *sufficient* for achieving closed loop stability. In the current case, given that γ_c is "large", $\gamma_c \cdot \gamma_F$ is probably larger than 1. Then,

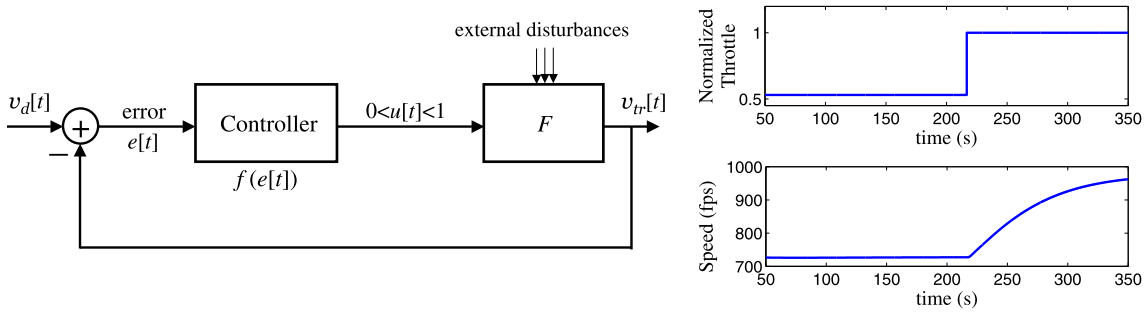

Fig. 5. The conceptual closed loop between desired and true ground speeds and the step response of the open loop block F.

given that the small gain theorem only provides a sufficient stability condition, either $e[t]$ continues to admit small, finite values, or $e[t]$ starts growing towards "large" values M. In this last (and worst case) scenario, the controller gain will become equal to $\gamma_c = \|\boldsymbol{u}\|/M \leq 1/M \ll 1$. At a given point, when $e[t]$ reaches some critical finite value e_{cr}, given that $\gamma_c < 1/e_{cr}$, the product $\gamma_c \cdot \gamma_F < 1$. Hence, by means of the small gain theorem, this is sufficient for achieving stability of the closed loop in Fig. 5, so that $e[t]$ starts decreasing again. Hence, $e[t] \leq e_{cr} < \infty$ in that case, too. The error $e[t]$ will also be bounded in case of uncertainties or disturbances present in the closed loop of Fig. 5. Then, the worst scenario for the case considered would be that the uncertainty or disturbance impact causes $e[t]$ to admit a large positive value M even faster than if such adverse factors were absent. Then, $\gamma_c \to 1/e_{cr}$ even faster than before and $\gamma_c \cdot \gamma_F < 1$, again. Note that the analysis via the small gain theorem is known to provide very conservative bounds. In other words, the analysis mainly indicates that (for that worst case scenario) the closed loop is still stable. If more details of the open loop system were available, convergence results (and less conservative bounds) could be obtained.

Now it remains to show that the signals involved in the closed loop system remain at least bounded. From (11), (15) and by means of standard calculus, J_t^{EXT} admits the following form:

$$\begin{aligned} J_t^{\text{EXT}} &= \left\|\boldsymbol{G}\cdot\boldsymbol{u}_t + (\boldsymbol{p}_t - \boldsymbol{r}_t)\right\|^2 + \mu\cdot\|\boldsymbol{D}\cdot\boldsymbol{u}_t - \boldsymbol{I_0}\|^2 \\ &\quad + \lambda_0[t]\cdot\|\boldsymbol{u}_t\|^2 + \lambda_1[t]\cdot\|\boldsymbol{I}_e - \boldsymbol{u}_t\|^2 \\ &= \|\boldsymbol{G}\cdot\boldsymbol{u}_t\|^2 + \|\boldsymbol{p}_t - \boldsymbol{r}_t\|^2 + 2\cdot(\boldsymbol{p}_t - \boldsymbol{r}_t)^T\cdot\boldsymbol{G}\cdot\boldsymbol{u}_t \\ &\quad + \mu\cdot\|\boldsymbol{D}\cdot\boldsymbol{u}_t\|^2 + \mu\cdot\|\boldsymbol{I_0}\|^2 \\ &\quad - 2\cdot\mu\cdot\boldsymbol{I_0}^T\cdot\boldsymbol{D}\cdot\boldsymbol{u}_t + \lambda_0[t]\cdot\|\boldsymbol{u}_t\|^2 + \lambda_1[t]\cdot\|\boldsymbol{I}_e\|^2 \\ &\quad + \lambda_1[t]\cdot\|\boldsymbol{u}_t\|^2 - 2\cdot\lambda_1[t]\cdot\boldsymbol{I}_e^T\cdot\boldsymbol{u}_t \end{aligned} \tag{18}$$

From (16) it follows that:

$$\begin{aligned} &\left(\boldsymbol{G}^T\boldsymbol{G} + \mu\cdot\boldsymbol{D}^T\boldsymbol{D} + \left(\lambda_0[t] + \lambda_1[t]\right)\cdot\boldsymbol{I}\right)\cdot\boldsymbol{u}_t \\ &\quad = \mu\cdot\boldsymbol{D}^T\boldsymbol{I}_0 + \lambda_1[t]\cdot\boldsymbol{I}_e + \boldsymbol{G}^T\cdot(\boldsymbol{r}_t - \boldsymbol{p}_t) \end{aligned} \tag{19}$$

Multiplying (19) by $\boldsymbol{u}_t^T$ yields:

$$\begin{aligned} &\boldsymbol{u}_t^T\cdot\left(\boldsymbol{G}^T\boldsymbol{G} + \mu\cdot\boldsymbol{D}^T\boldsymbol{D} + \left(\lambda_0[t] + \lambda_1[t]\right)\cdot\boldsymbol{I}\right)\cdot\boldsymbol{u}_t \\ &\quad = \boldsymbol{u}_t^T\cdot\left(\mu\cdot\boldsymbol{D}^T\boldsymbol{I}_0 + \lambda_1[t]\cdot\boldsymbol{I}_e + \boldsymbol{G}^T\cdot(\boldsymbol{r}_t - \boldsymbol{p}_t)\right) \end{aligned} \tag{20}$$

or

$$\begin{aligned} &\|\boldsymbol{G}\cdot\boldsymbol{u}_t\|^2 + \mu\cdot\|\boldsymbol{D}\cdot\boldsymbol{u}_t\|^2 + \left(\lambda_0[t] + \lambda_1[t]\right)\cdot\|\boldsymbol{u}_t\|^2 \\ &\quad = \boldsymbol{u}_t^T\cdot\left(\mu\cdot\boldsymbol{D}^T\boldsymbol{I}_0 + \lambda_1[t]\cdot\boldsymbol{I}_e + \boldsymbol{G}^T\cdot(\boldsymbol{r}_t - \boldsymbol{p}_t)\right). \end{aligned} \tag{21}$$

Combining (18) and (21), it follows:

$$\begin{aligned} J_t^{\text{EXT}} &= -\left((\boldsymbol{r}_t - \boldsymbol{p}_t)^T\cdot\boldsymbol{G} + \mu\cdot\boldsymbol{I_0}^T\cdot\boldsymbol{D} + \lambda_1[t]\cdot\boldsymbol{I}_e^T\right)\cdot\boldsymbol{u}_t \\ &\quad + \|\boldsymbol{p}_t - \boldsymbol{r}_t\|^2 + \mu\cdot\|\boldsymbol{I_0}\|^2 + \lambda_1[t]\cdot\|\boldsymbol{I}_e\|^2. \end{aligned} \tag{22}$$

Inserting (16) into (22) leads to:

$$\begin{aligned} J_t^{\text{EXT}} &= -\left((\boldsymbol{r}_t - \boldsymbol{p}_t)^T\cdot\boldsymbol{G} + \cdot\mu\cdot\|\boldsymbol{I_0}\|^T\cdot\boldsymbol{D} + \lambda_1[t]\cdot\boldsymbol{I}_e^T\right) \\ &\quad \cdot\left(\boldsymbol{G}^T\boldsymbol{G} + \mu\cdot\boldsymbol{D}^T\boldsymbol{D} + \left(\lambda_0[t] + \lambda_1[t]\right)\cdot\boldsymbol{I}\right)^{-1} \\ &\quad \cdot\left(\boldsymbol{G}\cdot(\boldsymbol{r}_t - \boldsymbol{p}_t) + \mu\cdot\boldsymbol{D}^T\cdot\boldsymbol{I_0} + \lambda_1[t]\cdot\boldsymbol{I}_e\right) + \|\boldsymbol{p}_t - \boldsymbol{r}_t\|^2 \\ &\quad + \mu\cdot\|\boldsymbol{I_0}\|^2 + \lambda_1[t]\cdot\|\boldsymbol{I}_e\|^2 \\ &= -\left\|\left\{\left(\boldsymbol{G}^T\boldsymbol{G} + \mu\cdot\boldsymbol{D}^T\boldsymbol{D} + \left(\lambda_0[t] + \lambda_1[t]\right)\cdot\boldsymbol{I}\right)^{-1}\right\}^{1/2}\right. \\ &\quad \left.\cdot\left(\boldsymbol{G}\cdot(\boldsymbol{r}_t - \boldsymbol{p}_t) + \mu\cdot\boldsymbol{D}^T\cdot\boldsymbol{I_0} + \lambda_1[t]\cdot\boldsymbol{I}_e\right)\right\|^2 \\ &\quad + \|\boldsymbol{p}_t - \boldsymbol{r}_t\|^2 + \mu + \lambda_1[t]\cdot n_{I_e}, \end{aligned} \tag{23}$$

with n_{I_e} the length of vector $\boldsymbol{I_e}$. By definition $J_t^{\text{EXT}} \geq 0$ for all t. Then, the quadratic term $\|\{(\boldsymbol{G}^T\boldsymbol{G} + \mu\cdot\boldsymbol{D}^T\boldsymbol{D} + (\lambda_0[t] + \lambda_1[t])\cdot\boldsymbol{I})^{-1}\}^{1/2}\cdot(\boldsymbol{G}\cdot(\boldsymbol{r}_t - \boldsymbol{p}_t) + \mu\cdot\boldsymbol{D}^T\cdot\boldsymbol{I_0} + \lambda_1[t]\cdot\boldsymbol{I}_e)\|^2$ is smaller than $\|\boldsymbol{p}_t - \boldsymbol{r}_t\|^2 + \mu + \lambda_1[t]\cdot n_{I_e}$ for all t. In order to investigate whether the signals in the controlled system stay bounded, one has to make sure that $J_t^{\text{EXT}} < \infty$ for all t. For this purpose two scenarios are considered:

Scenario a: The aircraft flies faster than it should, meaning that it will arrive earlier than planned at its next WP.

Scenario b: The aircraft flies slower than it should, meaning that it will arrive later than planned at its next WP.

When scenario a is valid, and given that the aircraft is "early", $\lambda_1[t] \to 0$, while $\lambda_0[t] \leq c_a\cdot e^{-c_b\cdot(v_d[t] - v_{tr}[t])} < \infty$ because $(v_d[t] - v_{tr}[t]) < 0$. Then (23) becomes:

$$\begin{aligned} J_t^{\text{EXT}} &\approx -\left\|\left\{\left(\boldsymbol{G}^T\boldsymbol{G} + \mu\cdot\boldsymbol{D}^T\boldsymbol{D} + \lambda_0[t]\cdot\boldsymbol{I}\right)^{-1}\right\}^{1/2}\right. \\ &\quad \left.\cdot\left(\boldsymbol{G}\cdot(\boldsymbol{r}_t - \boldsymbol{p}_t) + \mu\cdot\boldsymbol{D}^T\cdot\boldsymbol{I_0}\right)\right\|^2 + \|\boldsymbol{p}_t - \boldsymbol{r}_t\|^2 + \mu \end{aligned} \tag{24}$$

Note, that (24) could only grow unbounded with t if $\|\boldsymbol{p}_t - \boldsymbol{r}_t\| \to \infty$, due to $\|\boldsymbol{p}_t\|$ becoming very large with t. But from (9d), given that the identified ARX model is stable and that $\boldsymbol{u}_t$ in (16) is bounded (and decreasing when scenario a is valid), $\|\boldsymbol{p}_t\|$ could not grow to ∞. This is also reasonable because, when scenario a is valid, the aircraft will have to fly slower, thus achieving better SFC. The same conclusion is valid if disturbances or (modeling or other) uncertainties are present in the closed loop of Fig. 5. Then, the worst case under the scenario a would be that of the aircraft flying even faster than it should with respect to the given throttle command, so that $e[t] < 0$ with $|e[t]|$ growing. Again, the stable ARX model ensures that $\|\boldsymbol{p}_t\| < \infty$, because the throttle commands would be reduced even further by the controller. Hence, when scenario a is valid $J_t^{\text{EXT}} < \infty$ in time.

When scenario b is valid, then $\lambda_0[t] \to 0$ whereas $\lambda_1[t] \leq c_a\cdot e^{c_b\cdot(v_d[t] - v_{tr}[t])}$ with $(v_d[t] - v_{tr}[t]) > 0$. As demonstrated earlier on, $(v_d[t] - v_{tr}[t]) \leq e_{cr}$, meaning that $\lambda_1[t] \leq c_a\cdot e^{c_b\cdot e_{cr}} < \infty$ for all t. Then (24) could only grow unbounded with t if $\|\boldsymbol{p}_t - \boldsymbol{r}_t\| \to \infty$. Actually, since the aircraft is "late" when scenario b is valid, from (16) $\boldsymbol{u}_t$ will grow with time and, given that $y[t]$ in (9d) is provided by a stable linear ARX model, $y[t]$ (and $\|\boldsymbol{p}_t\|$) will grow too.

Let t^* be the critical instant after which $\boldsymbol{u}_t$ starts increasing. Consider $t > t^*$, for which $\|\boldsymbol{p}_t - \boldsymbol{r}_t\| \to M_t$, with M_t a possibly large number. Then for $t, t+1, \ldots$ the numbers $M_t, M_{t+1}, \ldots$ will form an increasing sequence, which, nonetheless, cannot escape to ∞ in finite time since $y[t]$ in $\boldsymbol{p}_t$ is provided by a linear stable ARX model. Again for $t > t^*$ and using (23) the values of J_t^{EXT} will approximately be as follows:

$$\begin{aligned} J_t^{\text{EXT}} \approx & -\Big\| \Big\{ \big(\boldsymbol{G}^T \boldsymbol{G} + \mu \cdot \boldsymbol{D}^T \boldsymbol{D} + \lambda_1[t] \cdot \boldsymbol{I} \big)^{-1} \Big\}^{1/2} \\ & \cdot \big(\boldsymbol{G} \cdot (\boldsymbol{r}_t - \boldsymbol{p}_t) + \mu \cdot \boldsymbol{D}^T \cdot \boldsymbol{I_0} + \lambda_1[t] \cdot \boldsymbol{I}_e \big) \Big\|^2 \\ & + \|\boldsymbol{p}_t - \boldsymbol{r}_t\|^2 + \mu + \lambda_1[t] \cdot n_{I_e} \\ \leq & -K_t \cdot \big(M_t^2 + \mu + c_a \cdot e^{c_b \cdot e_{cr}} \cdot n_{I_e} \big) \\ & + M_t^2 + \mu + c_a \cdot e^{c_b \cdot e_{cr}} \cdot n_{I_e}, \end{aligned} \tag{25}$$

with $K_t < 1$ positive numbers depending on $\lambda_0[t]$ and the norms of $\boldsymbol{G}$ and $\boldsymbol{D}$. Thus, J_t^{EXT} will start growing. Nonetheless, since for $t > t^*$ $\boldsymbol{u}_t$ is growing, the aircraft will fly faster and, inevitably, for some $t > t_{cr}$ (with $t_{cr} > t^*$ a specific finite time point), the aircraft will exceed the desired ground speed $u_d[t]$ and it will again be "early" with respect to its planned arrival time at the next WP. Thus, scenario b will no longer be valid, meaning that the aircraft will fly according to scenario a. Then again, $\boldsymbol{u}_t$ will start decreasing and the values of $J_t^{\text{EXT}} < \infty$ as demonstrated earlier on. Note that if disturbances or (modeling or other) uncertainties are present in the closed loop of Fig. 5, then the worst case under the considered scenario b would be that their impact hinders the aircraft acceleration so that an even bigger throttle command would be required for achieving the given speed. Then, for $t > t^*$ again $\|\boldsymbol{p}_t\| \to M_t$ and an increasing sequence $M_t, M_{t+1}, \ldots$ would be formed, as previously described. The difference is that, due to the hindered acceleration, the time instant t_{cr} will now arrive later meaning that the value $M_{t_{cr}}$ will be larger than before, but still bounded for the reasons explained earlier. Hence, in all cases $J_t^{\text{EXT}} < \infty$ and the signals involved cannot grow unbounded, meaning that the stability of the controlled system is achieved.

Remark. As previously shown, closed loop stability is obtainable even in presence of disturbances (or uncertainties) in Fig. 5. But, closed loop robustness will be challenged, although the proposed controller performs better than alternatives (see Section 3). In other words, the performance of the controller will be affected under such conditions. One way to attenuate their impact is to use disturbance observer schemes [25,26]. These utilize any known characteristics (describing functions, for instance) of the disturbance-entering channels, along with assumptions on the disturbance rate of change in order to estimate disturbance and other uncertainties. Then, this knowledge is used to filter out the disturbance impact on the signals involved in the MPC law and, thus, effectively enhance robustness of the closed loop. In the current case, disturbance observers could be used in an effective manner, provided that assumptions on disturbances caused by turbulence or sudden wind gusts would be available.

3. Simulation results

3.1. Identification of the relationship between throttle command and SFC

The identification of an ARX model representing the relationship between throttle command and engine SFC utilizes data from a simulated Boeing 737 implemented in the open source JSBSim simulator [12]. The same aircraft is used for implementing the designed controller. The flights considered for the ARX model identification procedure feature constant altitude, speed and heading, whereas no turbulence, gusts or winds are present. They cover a wide range of altitudes (from 1000 to 36 000 ft) with the duration of each flight equal to 180 seconds, and data recorded at a sampling rate $f_s = 20$ Hz. Initial position and control inputs of the aircraft are provided via a trimming function of the flight simulator. The throttle commands used for these flights are selected as resulting from a low-pass filtered Gaussian noise, whose mean value is the throttle control value obtained from the trimming function for the specific flight. This is done for properly exciting the engine dynamics and ensure identifiability of the relationship between throttle command and SFC.

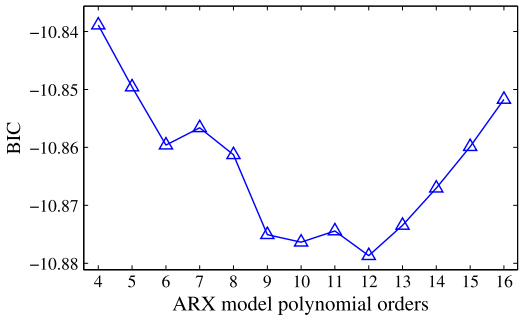

Fig. 6. Bayesian Information Criterion (BIC) order selection criterion for ARX(n, n) models.

The ARX identification procedure involves fitting ARX(na, nb) models of successively increasing orders na and nb to the available throttle and SFC data, with each such model evaluated by means of the Bayesian Information Criterion (BIC) [17, pp. 505–507]. A plot of BIC values computed using ARX(na, nb) models for growing values of na and nb is shown in Fig. 6. The minimal value of BIC indicates the optimal na, nb values for which the associated ARX(na, nb) achieves effective representation of the modeled dynamics (see Fig. 6). Hence, an adequate trade-off between accurate representation of the considered dynamics and limited number of ARX terms in $\boldsymbol{\theta}$ [see (4)] may be obtained. In the current case, the minimal BIC value is obtained for $na = nb = 12$. Finally, the selected ARX model is validated by checking the correlation of its residuals $w[t]$ [see (4)]. Lack of correlation among values of residuals $w[t]$ indicates that all meaningful information has been accounted for by the ARX model, with residuals resembling to white noise. The procedure for checking lack of correlation is standard and is presented in detail in [17, pp. 511–513]. It is based on the autocorrelation function describing the dependency between $w[t]$ and past (lagged) values $w[t-i]$. The estimated values of the autocorrelation for several (50–100) lags are plotted on a single chart along with statistical upper and lower bounds, which depend on the confidence level of the autocorrelation estimation (typically 95 or 99%). Sequence $w[t]$ is concluded as statistically uncorrelated if almost all plotted values are inside the bounds. Fig. 7 shows some representative results of the ARX$(12, 12)$ identification. Specifically, Fig. 7(a) presents an autocorrelation chart based on residuals $w[t]$ from the ARX$(12, 12)$ model for a flight evolving at 24 000 ft. Almost all autocorrelation values lie within the 95% confidence bounds (horizontal dashed lines), thus stating that the ARX$(12, 12)$ model is successfully validated. An additional pole-zero plot shown in Fig. 7(b) confirms that the model is both stable and minimum-phase, as its poles and zeros are located within the unit circle. Furthermore, Fig. 7(c) shows an example from actual SFC values for a flight evolving at 24 000 ft versus the SFC values predicted by the identified ARX$(12, 12)$ model during 200 time samples. Clearly, the predicted SFC values are always very close to the actual ones, thus demonstrating the ARX$(12, 12)$ prediction capabilities.

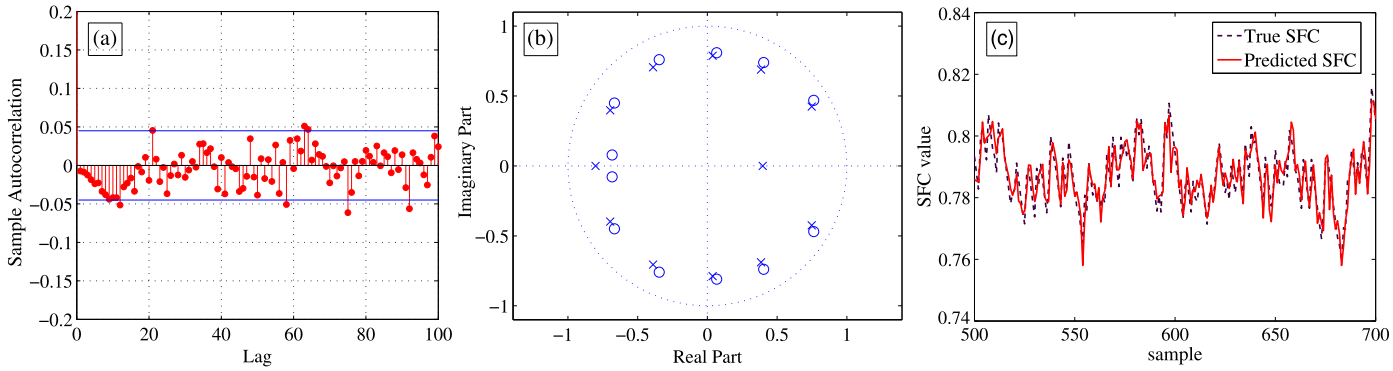

Fig. 7. (a) Autocorrelation function of the ARX(12, 12) model's one-step-ahead prediction error (residuals), (b) pole-zero plot of the selected ARX model and (c) example of actual versus ARX(12, 12)-predicted SFC values during 200 time samples of a flight at 24 000 ft.

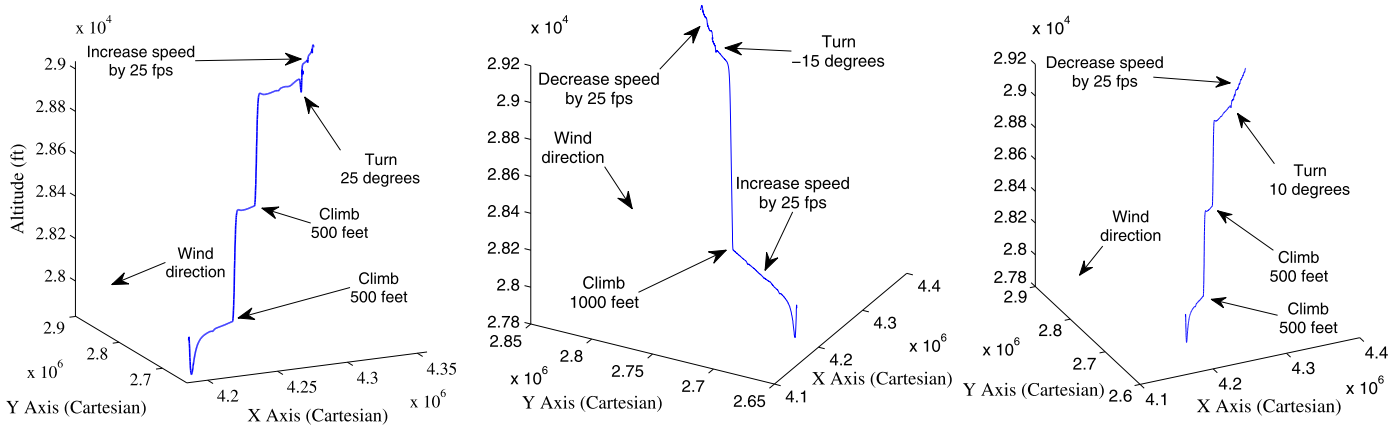

Fig. 8. Simulated B737 flight trajectories on 3-D space for the three assessment scenarios.

3.2. Controller assessment

The proposed GPC-based controller is compared with a traditional PID on various simulated cruise scenarios involving turbulence and/or wind. The tuning of the PID controller for ensuring 4DCo compliance was achieved via a two-stage iterative optimization approach, as the open loop transfer function of the aircraft dynamics was unavailable (see also Subsection 2.4). In the first stage the initial gains of the PID were determined via the Ziegler–Nichols method. Then, in the second stage, a trial-and-error optimization approach was employed based on which the refinement of the controller gains was achieved. Note that these flights are different with respect to those conducted for the ARX identification. They have a duration of 16 minutes and, as shown in Fig. 8, involve three 4DCos featuring:

(i) A climb of 1000 feet at time $t = 350$ s, a turn of 25 degrees at $t = 630$ s, and an increase of speed by 25 fps at $t = 880$ s.
(ii) An increase of speed by 25 fps at time $t = 350$ s, a climb of 1000 feet at $t = 530$ s, a turn of -15 degrees at $t = 630$, and an decrease of speed by 25 fps at $t = 880$ s.
(iii) A climb of 1000 feet at time $t = 350$ s, a turn of 10 degrees at $t = 630$ s, and an decrease of speed by 25 fps at $t = 880$ s.

Different flight cases correspond to different initial altitude and speed values (see Table 1), and are obtained via the trimming function of the JSBSim simulator. Note that, regardless of the wind/turbulence conditions used in each simulated flight, the throttle commands (16) are delivered using the identified ARX model obtained for turbulence- and wind-free flights carried out at an altitude comparable to that of the considered fight case. Apart from being realistic, this practice allows for testing the robustness of the proposed controller, since this is expected to perform adequately even under wind/turbulence conditions, for which it was not optimized. Again, following the same guidelines, the reference SFC value $\boldsymbol{r}_t$ in (16) should correspond to flights conducted under conditions which do not involve abrupt maneuvering, sudden wind gusts or significant turbulence. Then, the system should respect these SFC values, if possible also in case of degraded conditions (significant turbulence/winds). Therefore, as reference SFC values we consider those recorded during a single simulation carried out at an altitude comparable to that of the considered fight case, with initial commands and speed values given by the trimming function of the JSBSim simulator. Naturally, any other user-defined references, (for instance, data from past flights available in flight company databases) are also appropriate. Thus, the SFC should reach this representative (rather than minimal) value under the commands of the proposed auto-throttle, while aircraft 4DCo compliance and robustness under unexpected flight conditions should be maintained.

Table 1
Simulated flight cases for the comparison of GPC-based and PID controllers.

Flight case	Altitude (ft)	Ground speed (fps)
1	24 000	661
2	24 000	737
3	26 000	696
4	26 000	756
5	28 000	725
6	28 000	775
7	31 000	741

The user defined tuning parameters of the controller are determined as $c_a = 1$, $c_b = 0.3$, $\mu = 200$ and $j = 30$ samples (1.5 s), by a trial-and-error procedure.

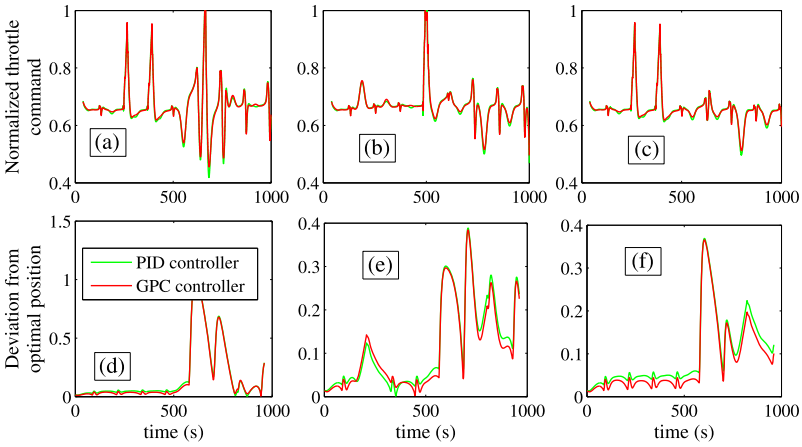

Fig. 9. Throttle commands (a), (b) and (c) correspond to 4DCos i, ii, and iii, respectively (see Fig. 8) and corresponding deviations (d), (e) and (f) (below) with respect to aircraft's 4DCo of the two controllers in absence of turbulence.

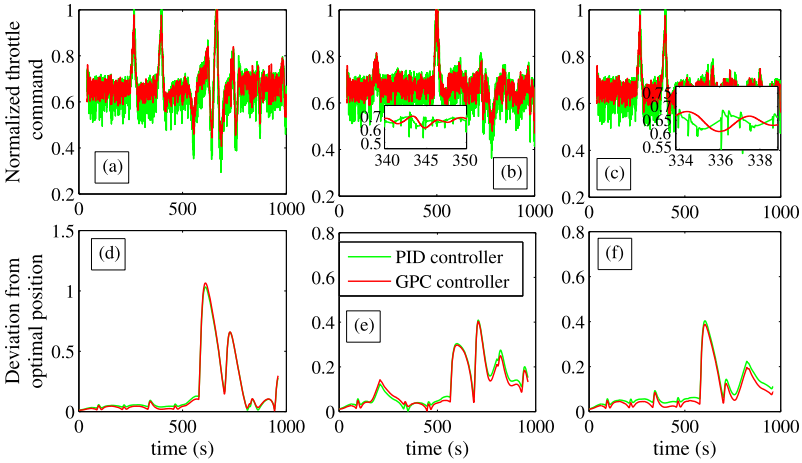

Fig. 10. Throttle commands (a), (b) and (c) correspond to 4DCos i, ii, and iii, respectively (see Fig. 8) and corresponding deviations (d), (e) and (f) (below) with respect to aircraft's 4DCo of the two controllers in presence of turbulence of type A.

Fig. 9 presents the comparison of the GPC- and PID-based controllers for an indicative cruise flight (flight case 7 in Table 1) with wind gusts but no turbulence. Figs. 9(a), 9(b), and 9(c) depict the throttle command obtained by the two controllers for the three 4DCo cases. It is clear that both controllers produce almost identical throttle commands under turbulence-free conditions. Figs. 9(d), 9(e), and 9(f) present the 4DCo deviations for the same flight and corresponding 4DCos. Again, both controllers achieve compliance of the aircraft with the assigned 4DCo, although the currently proposed auto-throttle controller slightly outperforms that based on the PID. The results of Fig. 9 are an indication that the two-stage iterative tuning approach of the PID controller, even suboptimal, results in an almost identical throttle command when compared to the GPC-based controller in turbulence-free flights. Fig. 10 presents comparative results for the same flight case as before, but this time under type A (that is, limited) turbulence, as provided by the simulator. In this case, the command outputs of the two controllers are quite different. It is clear that both controllers are affected by turbulence, since they were not tuned for achieving optimal operation under such conditions. Nonetheless, the GPC-based provides significantly smoother throttle commands than the controller based on the PID, with the latter exhibiting high-frequency oscillations. In the case of type B (that is, significant) turbulence (Fig. 11), the operation of the PID based controller deteriorates notably, with even more significant high-frequency oscillations. On the contrary, the proposed GPC-based controller is almost not affected at all. Overall, the GPC-based is quite more robust than the PID auto-throttle system in presence of turbulence. Although the throttle commands of the controllers differ significantly, their performance regarding the aircraft deviations with respect to the 4DCo is quite similar. Nevertheless, any throttle activity like the one exhibited by the PID based controller in Fig. 10 and 11 may not be considered as implementable and could constitute a threat for the system's long term reliability.

The marked difference in the control activity of the throttle command is less prominent for turbulence-free flights. This fact designates the proposed controller as more robust compared with classical solutions under flight conditions that the controller was not designed for (turbulence). Furthermore, note that both controllers achieved SFC values very close to the references. In other words, if realistic SFC values are set as references, the operational advantage of the proposed auto-throttle in its current application is related to achieving accurate 4DCo compliance, enhanced robustness and smoother throttle activity with respect to classical alternatives (PID). Work is currently underway for achieving meaningful reduction of SFC coupled to 4D Contract compliance.

Remark. The technical details for implementing the proposed controller are obviously related to the aircraft under consideration. At this stage, given that the controller is implemented in a simulated 737, the technical problems related to the actual hardware implementation are hard to identify. On a conceptual basis, however, the biggest issue stems from the fact that a dependable SFC estimate has to be obtained on-board, for instance by the FADEC system, as

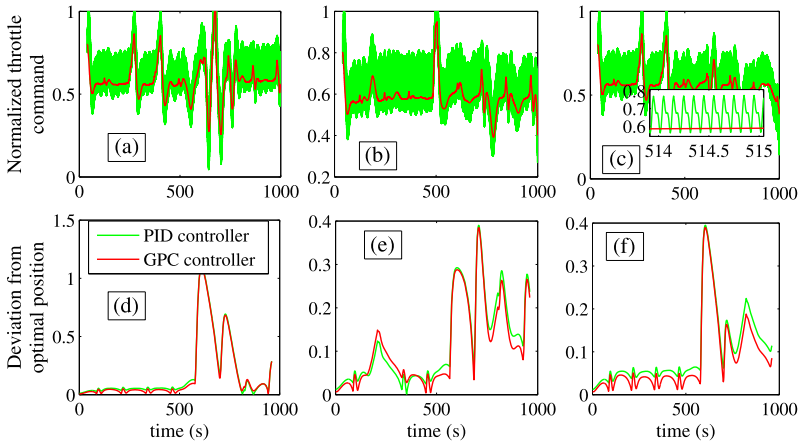

Fig. 11. Throttle commands (a), (b) and (c) correspond to 4DCos i, ii, and iii, respectively (see Fig. 8) and corresponding deviations (d), (e) and (f) (below) with respect to aircraft's 4DCo of the two controllers in presence of turbulence of type B.

claimed in [18]. If this is not the case, a dependable thrust estimate has to be obtained on-board, using, for instance, the estimation filters in [10]. On the other hand, the actual on-board resources dedicated to the calculation of the throttle commands are, indeed, minimal because the latter is obtained via a closed-form solution. In any case, the technical implementation of the proposed controller should be included in a dedicated case study, and as such it cannot be the object of the current work.

4. Conclusions

A novel auto-throttle controller aiming at simultaneously obtaining safe aircraft positioning in 4DCo flight and achieving reasonable fuel use (in terms of SFC) has been presented. The controller design is formulated as a model (and, specifically, generalized) predictive control problem, with its solution providing the throttle command. The innovation resides in the fact that two objectives are achieved when computing the auto-throttle command: Respecting some designated SFC reference values and complying with the assigned 4DCo. Due to the identification of a linear stochastic ARX representation for the relationship between throttle command and SFC, the formulation of a generalized predictive control problem is enabled. Thus, in the present case an analytical closed-form solution to the GPC problem providing the throttle command is obtainable. This is beneficial for the controller's on-board implementation, since no extra computational burden is imposed. Comparisons via simulated flights with a conventional PID controller show that the proposed solution is more robust under demanding conditions (turbulence), while achieving an improvement in terms of aircraft 4DCo compliance. Overall, in the current case, emphasis was not given to the absolute SFC minimization, but rather its regulation to a reasonable benchmark value. Absolute SFC minimization is the objective of future work.

Conflict of interest statement

No conflict of interest exists.

Acknowledgements

Research supported by the European Commission – FP7 Project No. 266296 4DCo-C ("4 Dimension Contracts – Guidance and Control").

References

[1] L.C. Andrews, Special Functions of Mathematics for Engineers, SPIE Press, 1998, pp. 110–111.
[2] K.J. Astrom, R.M. Murray, Feedback Systems: An Introduction for Scientists and Engineers, Princeton University Press, Princeton and Oxford, 2009, pp. 287–355.
[3] B.J. Brunell, Methods and apparatus for model predictive control of aircraft gas turbine engines, Patent US 6823253, 2004.
[4] J.W. Burrows, Fuel optimal trajectory computation, J. Aircr. 19 (4) (1982) 324–329.
[5] E.F. Camacho, D. Bordons, Model Predictive Control in the Process Industry, Springer-Verlag, London, 1995.
[6] D.W. Clarke, C. Mohtadi, P.S. Tuffs, Generalized predictive control – Part I. The basic algorithm, Automatica 23 (2) (1987) 137–148.
[7] X. Dai, T. Breikin, Z. Gao, H. Wang, Dynamic modelling and robust fault detection of a gas turbine engine, in: American Control Conference, Seattle, Washington, USA, June 2008, pp. 11–13.
[8] A. Franco, D. Rivas, Minimum-cost cruise at constant altitude of commercial aircraft including wind effects, Engineering Notes, J. Guid. Control Dyn. 34 (4) (2011) 1253–1260.
[9] A. Franco, D. Rivas, Analysis of optimal aircraft cruise with fixed arrival time including wind effects, Aerosp. Sci. Technol. 32 (1) (2014) 212–222, http://dx.doi.org/10.1016/j.ast.2013.10.005.
[10] M. Henriksson, T. Gronstedt, C. Breitholtz, Model-based on-board turbofan thrust estimation, Control Eng. Pract. 19 (2011) 602–610.
[11] J.K. Huusom, N.K. Poulsen, S.B. Jorgensen, J.B. Jorgensen, Tuning methods for offset free MPC based on ARX Model representations, in: American Control Conference, Baltimore, MD, USA, June 30–July 02, 2010.
[12] http://jsbsim.sourceforge.net/, last accessed on March 11, 2014.
[13] A. Joulia, Four dimensional contracts guidance and control, European project document "4DCo-GC2-AnnexI_v1_2".
[14] H.S. Khalil, Nonlinear Systems, 3rd ed., Prentice Hall, Upper Saddle River, New Jersey, 2002, p. 217.
[15] A. Kreiner, K. Lietzau, The use of onboard real-time engine models for jet engine control, Technical Report, MTU Aero Engines, Germany, 2003.
[16] W.S. Levine, The Control Handbook, CRC–IEEE Press, Boca Raton, FL, 2000, p. 808.
[17] L. Ljung, System Identification: Theory for the User, 2nd edn., PTR Prentice Hall, Upper Saddle River, NJ, 1999.
[18] R.H. Luppold, Apparatus and method for reducing aircraft fuel consumption, Patent US 20110202251, 2011.
[19] O.D. Lyantsev, Synthesis of nonlinear optimal real-time automatic control systems for gas turbine engines, J. Comput. Syst. Sci. Int. 46 (3) (2007) 484–492.
[20] O.D. Lyantsev, T.V. Breikin, G.G. Kulikov, V.Y. Arkov, On-line performance optimisation of aero engine control system, Automatica 39 (2003) 2115–2121.
[21] J. Maciejowski, Predictive Control with Constraints, Pearson Education Limited, Harlow, England, 2002.
[22] M. Montazeri-Gh, S. Jafari, M.R. Ilkhani, Application of particle swarm optimization in gas turbine engine fuel controller gain tuning, Eng. Optim. 44 (2) (2012) 225–240.
[23] J.A. Sorensen, M.H. Waters, Airborne method to minimize fuel with fixed time-of-arrival constraints, J. Guid. Control Dyn. 4 (1981) 348–349.
[24] H.A. Spang, H. Brown, Control of jet engines, Control Eng. Pract. 7 (1999) 1043–1059.
[25] J. Yang, W.X. Zheng, Offset-free nonlinear MPC for mismatched disturbance attenuation with application to a static Var compensator, IEEE Trans. Circuits Syst. II, Express Briefs 61 (1) (2014) 49–53.
[26] J. Yang, Z. Zhao, S. Li, W.X. Zheng, Composite predictive flight control for air-breathing hypersonic vehicles, Int. J. Control 87 (9) (2014) 1970–1984.